Leukemia (2008) 22, 1131–1138

www.nature.com/leu

ORIGINAL ARTICLE

RNAi-mediated silencing of p190$^{Bcr\text{-}Abl}$ inactivates Stat5 and cooperates with imatinib mesylate and 17-allylamino-17-demetoxygeldanamycin in selective killing of p190$^{Bcr\text{-}Abl}$-expressing leukemia cells

M Futami[1], T Hatano[2], Y Soda[1], S Kobayashi[1], M Miyagishi[3] and A Tojo[1]

[1]*Division of Molecular Therapy, Advanced Clinical Research Center, Institute of Medical Science, University of Tokyo, Tokyo, Japan;* [2]*Department of Chemistry and Biotechnology, School of Engineering, University of Tokyo, Tokyo, Japan and* [3]*The 21st Century Center of Excellence (COE) Program, Graduate School of Medicine, University of Tokyo, Tokyo, Japan*

The 190 kD (p190) and 210 kD (p210) Bcr-Abl proteins are responsible for the pathophysiology of Philadelphia chromosome (Ph)$^+$ leukemia. We applied RNA interference (RNAi) to specific killing of p190$^+$ cells, and determined the optimal sequences for gene silencing in the BCR, junctional and ABL regions of p190, respectively. Then, p190$^+$ and p210$^+$ cells were infected with lentiviral vectors encoding these shRNAs, resulting in efficient killing of p190$^+$ cells, while p210$^+$ cells were only sensitive to shBCR and shABL. In p190-transformed Ba/F3 cells, silencing of p190 specifically inhibited tyrosine phosphorylation of Stat5 prior to their death, but did not affect phosphorylation of Jak2, Akt or MEK1/2. In contrast, downregulation of p190 by their treatment with 17-allylamino-17-demetoxygeldanamycin (17-AAG) was associated with reduced protein levels of Jak2, Akt and MEK1/2. shRNA targeting p190 collaborated additively with imatinib and 17-AAG in growth inhibition of Ba/F3-p190wt and imatinib-resistant Ba/F3-p190Y253H cells. Collectively, RNAi-mediated silencing of p190 is a promising option both for delineating signal transduction and for therapeutic application in 190$^+$ leukemia.
Leukemia (2008) **22**, 1131–1138; doi:10.1038/leu.2008.60;
published online 27 March 2008
Keywords: Bcr-Abl; Ph$^+$ALL; RNAi; lentiviral vector; 17-AAG; Stat5

Introduction

Philadelphia chromosome (Ph)$^+$ leukemia, including chronic myeloid leukemia (CML) and acute lymphoblastic leukemia (Ph$^+$ALL), originates from hematopoietic stem/progenitor cells affected by the BCR-ABL fusion gene, which encodes constitutively active tyrosine kinase essential for development and progression of the diseases.[1] There are two major forms of Bcr-Abl protein, p210 and p190. The former is associated with almost all cases of CML and less than half of Ph$^+$ALL cases, whereas the latter mainly causes Ph$^+$ALL except for very rare cases of CML.[2]

The development of imatinib (also referred to as STI571), and the second generation tyrosine kinase inhibitors have greatly improved the clinical outcome of CML.[3–5] However, Ph$^+$ALL shows a much less durable response to these kinase inhibitors, and easily acquires resistance, caused primarily by point mutations in the Abl kinase domain such as T315I.[6,7] To overcome the resistance, the downregulation of Bcr-Abl proteins is a promising strategy for eliminating Ph$^+$ALL cells, irrespective of point mutations. From this viewpoint, we have previously reported that lentiviral delivery of anti-p190 maxizyme specifically induces apoptosis in Ph$^+$ALL cells.[8]

Recently, RNA interference (RNAi) has been recognized as a more powerful tool in the selective gene silencing. RNAi allows downregulation of target genes at the post-transcriptional level via sequence-specific mRNA depletion. This can be accomplished by the delivery of double-strand RNA in the form of small interfering RNA (siRNA) or small hairpin RNA (shRNA).[9,10] Anti-p210 RNAi targeting sequences of the junctional domain of Bcr-Abl suppressed its expression in CML cell lines, resulting in growth inhibition,[11,12] and lentivirus-mediated stable expression of anti-p210 shRNA has also been successful.[13,14] Similarly, electroporation of p190$^+$ cells with anti-p190 siRNA downregulated p190 and reduced cell viability in a dose-dependent fashion.[15] However, this procedure may exert nonspecific toxicity on intact cells, and short-lived siRNA is not suitable for monitoring cell viability. Therefore, to precisely evaluate the consequences of RNAi-mediated p190 silencing, viral vector-mediated transfer and stable expression of shRNA in p190$^+$ cells are required.

In the present study, we successfully downregulated p190 by lentiviral transduction with shRNA targeting p190, resulting in efficiently killing of p190$^+$ cells. We also observed that silencing of p190 caused specific inactivation of Stat5 and cooperated with imatinib and 17-allylamino-17-demetoxygeldanamycin (17-AAG) in the selective killing of p190$^+$ cells.

Materials and methods

Design of shRNAs targeting p190

Three types of 21-bp shRNA were designed, and named as shE1A2, shABL and shBCR, respectively. shE1A2 targets junctional lesion between BCR exon 1 and ABL exon 2 (e1a2) in p190 mRNA. The sequence was determined after the screening by a transient transfection of 293/p190 cells with a series of U6-promoter driven shE1A2 expression vectors, in which we found that the center of junctional lesion was suitable for target site (Supplementary Figure 1). We also designed shABL targeting nt 1238–1258 of ABL, and shBCR targeting nt 992–1012 of BCR, with a computer algorithm (iGENE Therapeutics, Tsukuba, Japan) to identify optimal sequences, and tested for their ability to downregulate p190 (Supplementary Figure 2). shLUC targeting *Renilla* luciferase was prepared as a control. Although shE1A2 is supposed to be specific for p190, shABL is

Correspondence: Dr A Tojo, Division of Molecular Therapy, Advanced Clinical Research Center, Institute of Medical Science, University of Tokyo, 4-6-1 Shirokanedai, Munato-ku, Tokyo 108-8639, Japan.
E-mail: a-tojo@ims.u-tokyo.ac.jp
Received 26 August 2007; revised 18 February 2008; accepted 19 February 2008; published online 27 March 2008

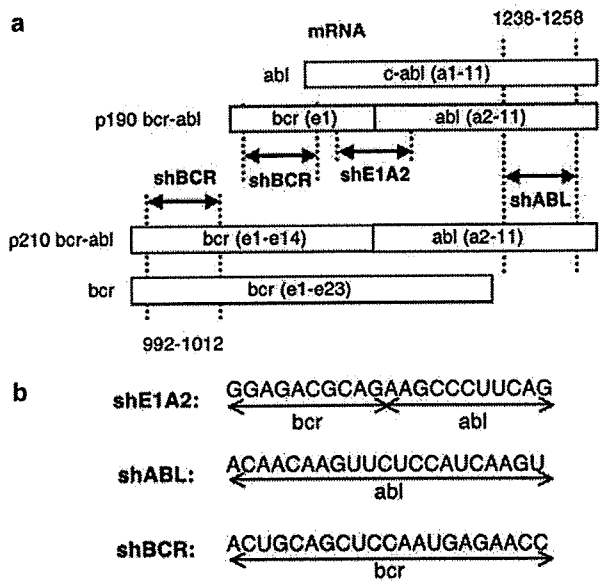

Figure 1 Target sites for shRNAs. (**a**) Locations of target site. Arrows indicate the target sites of shRNAs on abl, e1a2 of p190 Bcr-Abl, e14a2 of p210 Bcr-Abl and bcr mRNA. (**b**) The target site sequences. Arrows indicate areas in which the sequence is complementary to that of bcr or abl.

predicted to affect not only p190 but also p210 and Abl. Similarly, shBCR is predicted to affect p190, p210 as well as Bcr (Figures 1a and b).

Production of lentiviral vectors

The nucleotide sequences of the shRNA expression cassette in the piGENE-PURhU6/shRNA were amplified by polymerase chain reaction using Platinum *pfx* DNA polymerase (Invitrogen, Carlsbad, CA, USA) and a primer set containing a *Bam*HI site (forward 5′-ATGGATCCAAGGTCGGGCAGGAAGAGG-3′ and reverse 5′-ATGGATCCCATGATGATTACGCCAAGCTTGCAT-3′). The resulting fragments were digested with *Bam*HI and ligated into a *Bam*HI-digested self-inactivating lentiviral transfer vector. The expression cassettes for shE1A2, shABL and shLUC were inserted into lentiviral transfer vector pCS-CDF-EG-PRE containing elongation factor 1α (EF1α) promoter-driven human CD2 as a selection marker (pHIV-CD2), and the shBCR expression cassette was inserted into a similar transfer vector containing CD271 as a marker (pHIV-CD271). Lentiviral vector particles were produced by cotransfection of 293T cells with pHIV-hU6/shRNA, pMDLg/p.RRE, pRSV-rev and pMD.G as described previously.[16] Transduction efficiency was analyzed by flow cytometry of marker gene expression, resulting in 94–99% at high multiplicity of infection (MOI = 5) and around 50% (36–59%) at low MOI (MOI = 1).

Western blot analysis

Cells were lysed, and 50 μg of the lysate were electrophoresed in SDS-polyacrylamide gels, transferred onto polyvinylidene fluoride membranes, and blotted with the respective antibodies, according to the manufactures' instructions. All secondary antibodies were peroxidase-conjugated, and proteins were detected using enhanced chemiluminescence (Amersham, Arlington Heights, IL, USA). The following antibodies were

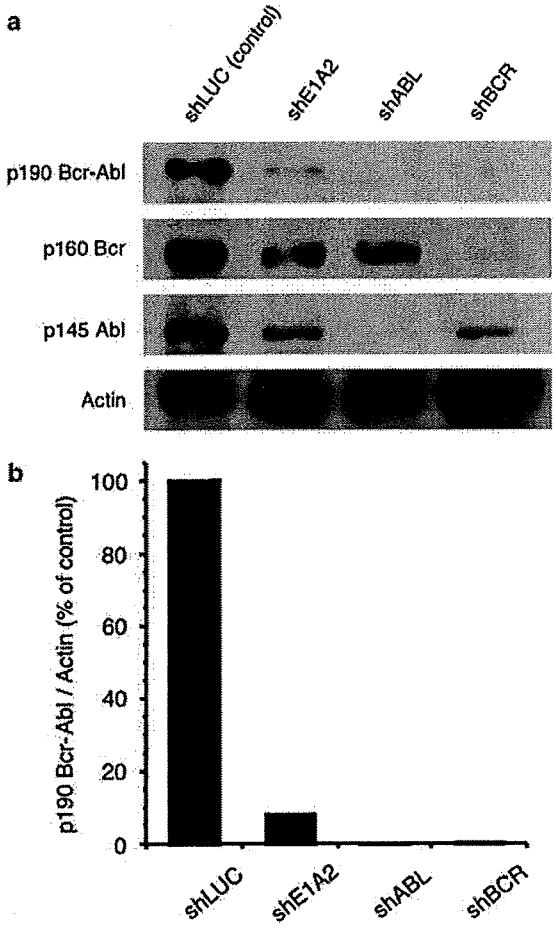

Figure 2 Lentivirus-mediated RNAi silences the expression of p190 Bcr-Abl. (**a**) HEK 293/p190 cells were transduced with shLUC (control), shE1A2, shABL and shBCR at an MOI of 5. The cells were lysed on day 3, and lysates were labeled with the respective antibodies: p190 Bcr-Abl and p145 Abl, with anti-Abl antibody; p160 Bcr, with anti-Bcr antibody and and actin, with anti-actin antibody. The transduction efficiencies, determined by FACS analysis of marker gene expression on day 3: shLUC, 99.1%; shE1A2, 99.3%; shABL, 96.9% and shBCR, 98.1%. (**b**) Quantitative analysis of p190 expression. Quantitative analysis was performed using NIH Image 1.63 (National Institutes of Health, Bethesda, MD, USA), and p190 levels were normalized by actin.

used: anti-Abl (8E9; BD Biosciences, San Diego, CA, USA), anti-Bcr (N-20; Santa Cruz Biotechnology, Santa Cruz, CA, USA), anti-Jak2 (06-255; Upstate Biotechnology, Lake Placid, NY, USA), anti-phospho-Jak2 (Tyr1007/1008; Upstate Biotechnology), and anti-Stat5 (C-17; Santa Cruz Biotechnology); anti-phospho-Stat5 (Tyr694), anti-Akt1, (2H10), anti-phospho-Akt (Ser473), anti-MEK1/2 (L38C12), anti-phospho-MEK1/2 (Ser221) (all from Cell Signaling Technology, Danvers, MA, USA); anti-Actin (AC-40; Sigma, St Louis, MO, USA), sheep anti-mouse IgG (515-036-072; Jacson ImmunoResearch Labolatories, West Grove, PA, USA) and donkey anti-rabbit IgG (NA934V; Amersham Biosciences, Little Chalfont, Bucks, UK).

Cell count and viability assay

Aliquots of 5×10^4 cells (10^5 cells for KOPN-30 cells) in 1 ml of culture medium were plated in a 24-multiwell plate. Cell

number and viability were determined by trypan blue dye exclusion. For cell proliferation assay, 10^3 cells in 100 µl of culture medium were grown in a 96-multiwell plate. Viable cell number was assessed on day 4 using WST-8 assay kit (Seikagaku, Tokyo, Japan).

Colony-forming assay

Human CD34$^+$ cells were purified from umbilical cord blood mononuclear cells by a two-round separation procedure using the Indirect CD34 MicroBead Kit (Miltenyi Biotec, Auburn, CA, USA). Purified CD34$^+$ cells were cultured in α-minimal essential medium containing 30% fetal bovine serum (FBS), 50 ng ml^{-1} hSCF, 50 ng ml^{-1} hTPO, 10 ng ml^{-1} hIL-3 and 50 ng ml^{-1} Flt3L for 24 h, transduced with anti-p190 shRNA lentiviral vectors at an MOI of 20, and incubated for 48 h. Aliquots of 10^3 transduced cells were plated in triplicate in 1 ml of 0.9% methylcellulose containing 30% FBS, 50 ng ml^{-1} hSCF, 10 ng ml^{-1} hIL-3, 100 ng ml^{-1} hG-CSF, and 2 U ml^{-1} hEPO. After 14 days, the number of each type of colony was scored.

Results

Silencing effect of anti-p190 shRNA lentiviral vectors

To confirm the silencing effect, we transduced HEK 293/p190 cells with lentiviral vectors encoding anti-p190 shRNA (shE1A2, shABL and shBCR) at an MOI of 5, and the expression level of p190 was determined by western blot analysis. p190 Bcr-Abl expression were substantially suppressed (0.0–8.0%) by these three anti-p190 shRNAs (Figures 2a and b). The expression of p145 Abl and p160 Bcr was substantially inhibited by shABL and shBCR, respectively (Figure 2a).

Proliferation and survival of leukemia cell lines after the transduction of shRNAs

To investigate the biological consequences of anti-p190 shRNAs, p190$^+$ KOPN-30 cells, p210$^+$ K562 cells and p190/p210$^-$ NALM-6 cells were infected with lentiviral vectors encoding these shRNAs at an MOI of 5, and cell proliferation and viability were determined by trypan blue dye exclusion. The Ph$^+$ALL-derived KOPN-30 p190$^+$ cells ceased proliferation at two days after transduction with shE1A2, shABL and shBCR, and decreased in cell number and viability in a time-dependent manner, confirming that shRNA-mediated downregulation of p190 can kill Ph$^+$ALL cells (Figure 3). Given that shABL and shBCR would be expected to knock down both p190 and p210, we assessed the effect of these shRNAs in K562 cells, which express p210. As expected, shABL and shBCR eradicated the K562 cells, whereas shE1A2 did not have a notable effect, indicating that shE1A2 is sequence-specific to p190 (Figure 3). To further confirm that RNAi-mediated downregulation is target sequence specific, we also transduced p190/p210$^-$ NALM-6 cells. None of the anti-p190 shRNAs affected survival in NALM-6 cells, although shABL appeared to have some inhibitory effect on growth, which suggests that p145 Abl may be positively involved in NALM-6 cell proliferation.

The effect of shRNAs on imatinib-resistant cells

To determine whether anti-p190 shRNAs overcome imatinib resistance, murine Ba/F3 cells transformed with wild-type p190 or imatinib-resistant mutant (p190Y253H) were transduced with shE1A2, shABL and shBCR. In the absence of IL-3, these shRNAs depleted BaF/3 cells with both types of p190 in an equipotent manner (Figure 4 left). Supplementation of IL-3 clearly rescued these cells from shRNA-mediated cytotoxic effects, suggesting that signal transduction machinery downstream of IL-3 receptor might be maintained irrespective of p190 expression (Figure 4 right).

The effect of downregulation of Abl and Bcr on normal hematopoiesis

We tested the effects of shABL and shBCR on cytokine-dependent clonal growth and differentiation of normal CD34$^+$ cells. Figure 4b shows that shBCR did not influence colony

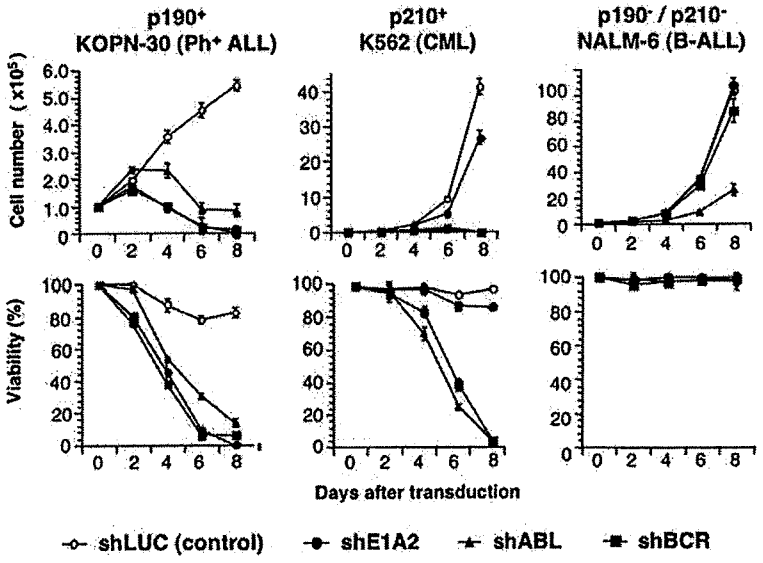

Figure 3 RNAi targeting the junctional domain of p190 kills specifically p190$^+$ cells; RNAi targeting Abl or Bcr kills both p190$^+$ cells and p210$^+$ cells. Cells were transduced with shLUC (control), shE1A2, shABL and shBCR at an MOI of 5. Cell number and viability was determined by the trypan blue exclusion.

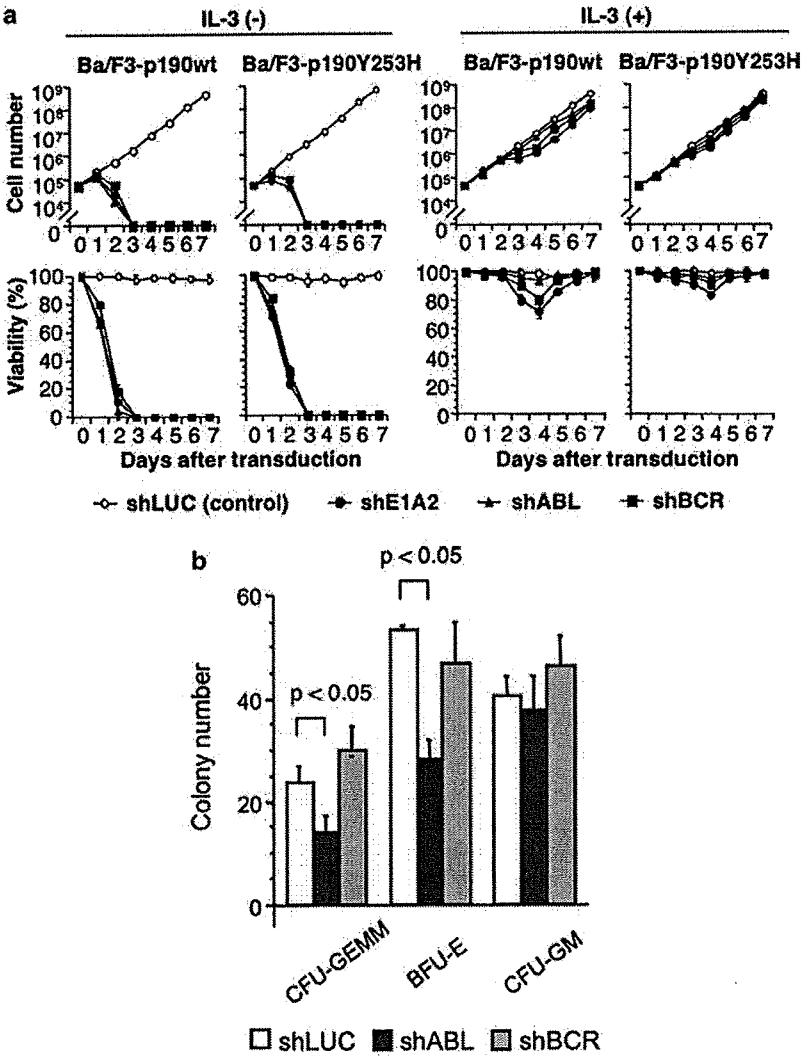

Figure 4 (a) Anti-p190 shRNAs kill BaF/3-p190 cells, and supplementation with IL-3 rescues these cells. Cells were transduced with shLUC, shE1A2, shABL and shBCR at an MOI of 5, and cultured in the absence or presence (10 ng ml^{-1}) of murine IL-3. Cell number and viability were determined by trypan blue exclusion. (b) Knock-down of Abl suppresses hematopoietic colony formation of normal cord blood CD34$^+$ cells. Cord blood CD34$^+$ cells were transduced with shRNA lentiviral vectors at an MOI of 20, and cytokine-dependent clonal growth was examined by the methylcellulose hematopoietic colony-forming assay. The number of various types of colonies was scored after 14 days in culture.

formation derived from colony-forming unit granulocyte-erythrocyte-monocyte-megakariocyte (CFU-GEMM), CFU granulocyte-monocyte (CFU-GM), and burst-forming unit erythroid (BFU-E) cells, but shABL markedly suppressed CFU-GEMM and BFU-E-derived colony formation.

The effect of Anti-p190 shRNA on p190 and the downstream signal transduction pathway

Bcr-Abl kinase activates a number of signal transduction pathways, including the Jak/Stat, PI3K/Akt and Ras/Raf/MEK/ERK pathways.[17] However, the relative contributions of these signaling pathways to p190-triggered proliferation and survival are not fully understood. To elucidate the primary event that is directly influenced by the downregulation of p190 Bcr-Abl, Ba/F3-p190wt cells were transduced with anti-p190 shRNAs, and the phosphorylation status of molecules involved in Bcr-Abl-mediated transformation was determined by immunoblot analysis at 48 h after transduction (Figure 5a). There were no significant changes in phosphorylation status of Jak2 by the treatment with anti-p190 shRNAs. In contrast, a marked reduction in phosphorylated Stat5 was noted in anti-p190 shRNA-treated BaF/3-p190wt cells, supporting the idea that p190 activates Stat5 in a Jak2-independent manner. Anti-p190 shRNAs did not significantly affect phosphorylation of Akt or MEK1/2. These results imply that downregulation of p190 rapidly results in the inactivation of Stat5, but inactivation of either PI3K/Akt or Ras/Raf/MEK/ERK pathway is not significant compared with Stat5.

The effect of 17-AAG on p190 and the downstream signal transduction pathway

Treatment with 17-AAG disrupts Hsp90 function and degrades its client protein, p190/p210.[18,19] Ba/F3-p190wt cells were treated with increasing concentrations of 17-AAG for 24 h, and

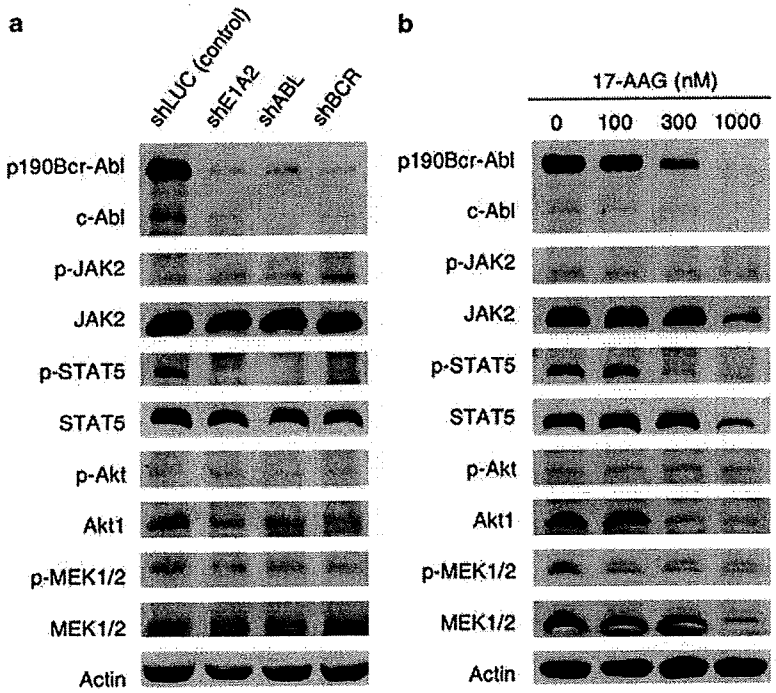

Figure 5 Western blot analysis of Ba/F3-p190wt cells. (**a**) Ba/F3-p190wt cells were transduced with shRNA lentiviral vectors at an MOI of 5. Cells were harvested at 48 h after transduction, lysed and labeled with the respective antibodies. (**b**) Ba/F3-p190wt cells were cultured in the presence or absence of 17-AAG (0–1000 nM) for 24 h. Lysates were labeled with the respective antibodies.

the expression level and phosphorylation status of the same molecules shown in Figure 5a were analyzed. As shown in Figure 5b, 17-AAG downregulated both p190 and p145 Abl in a dose-dependent manner at concentrations >300 nM. The Jak2 protein level was downregulated at 1000 nM. The downregulation of phosphorylated Stat5 preceded that of total Stat5 protein level, which was not affected by the treatment with 17-AAG up to 300 nM. Akt1 and MEK1/2 were downregulated by 17-AAG at around 300 nM. These results suggest that 17-AAG affects p190 as well as various molecules involved in Bcr-Abl-mediated transformation.

Combined effects between shRNA, imatinib and 17-AAG

Because anti-p190 RNAi and 17-AAG can downregulate p190 by different mechanisms, and imatinib inactivates the kinase activity of p190, their combination may work in a synergistic or additive manner in killing of Ba/F3-p190wt and BaF/3-p190Y253H cells. These two cell lines were transduced with anti-p190 shRNAs in a suboptimal condition (MOI = 1) and cultured with increasing dose of either imatinib or 17-AAG. Under these conditions, anti-p190 shRNAs increased sensitivity of Ba/F3-p190wt cells to imatinib and 17-AAG. BaF/3-p190Y253H cells did not respond to imatinib, even at 5 μM; however, the anti-p190 shRNAs appeared to restore sensitivity to higher concentrations of imatinib (Figure 6a). On the other hand, anti-p190 shRNAs cooperated with 17-AAG to kill Ba/F3-p190Y253H cells, with a dose-response curve similar to that in Ba/F3-p190wt cells (Figure 6b). When Ba/F3-p190 cells were exposed to various dosage combinations of 17-AAG and imatinib, the drugs acted synergistically to kill Ba/F3-p190wt cells, and 17-AAG clearly sensitized Ba/F3-p190Y253H cells to imatinib (Figure 6c).

Discussion

We applied RNAi to test whether specific and efficient killing of Ph$^+$ ALL cells could be achieved by downregulation of p190. Wohlbold *et al.*[15] first reported the effective inhibition of p190 protein by siRNA and its cytotoxicity in murine 32D-p190 cells; however, they induced siRNA by elecroporation, which is likely to cause nonspecific damage to recipient cells. We independently designed a series of overlapping shRNAs complementary to the e1a2 junction of p190 and determined the optimal target sequence for inhibition, finding a sequence identical to that described by Wohlbold *et al.* Use of lentiviral transfer of shRNA expression cassettes provided efficient transduction and sustained silencing of the target protein with reduced nonspecific damage. Using a similar vector system, Scherr *et al.*[14] have demonstrated that stable, but not transient, RNAi can efficiently deplete p210 from p210$^+$ cells, depending on the MOI used for infection; transduction at a high MOI resulted in almost complete loss of viable cells, but transduction at a low MOI caused minimal growth inhibition. These results are compatible with our data in Figures 4 and 6.

We also showed that shBCR and shABL very efficiently downregulated p190/p210 Bcr-Abl proteins as well as their normal counterparts. Although Abl-deficient mice have multiple defects, including high postnatal mortality, runting and morphological abnormalities, Abl is considered to be dispensable for the function of hematopoietic stem cells, myeloid progenitor cells and immune cells.[20,21] On the other hand, Bcr-null mice appear intact, and a peculiar finding is that their neutrophils show a marked increase in superoxide production upon activation.[22] Consistent with these findings, shABL slightly inhibited proliferation of p190/p210$^-$ NALM-6 cells without loss of viability, but shBCR did not affect these cells. In addition, BaF/3-p190 cells treated with shABL and shBCR could be

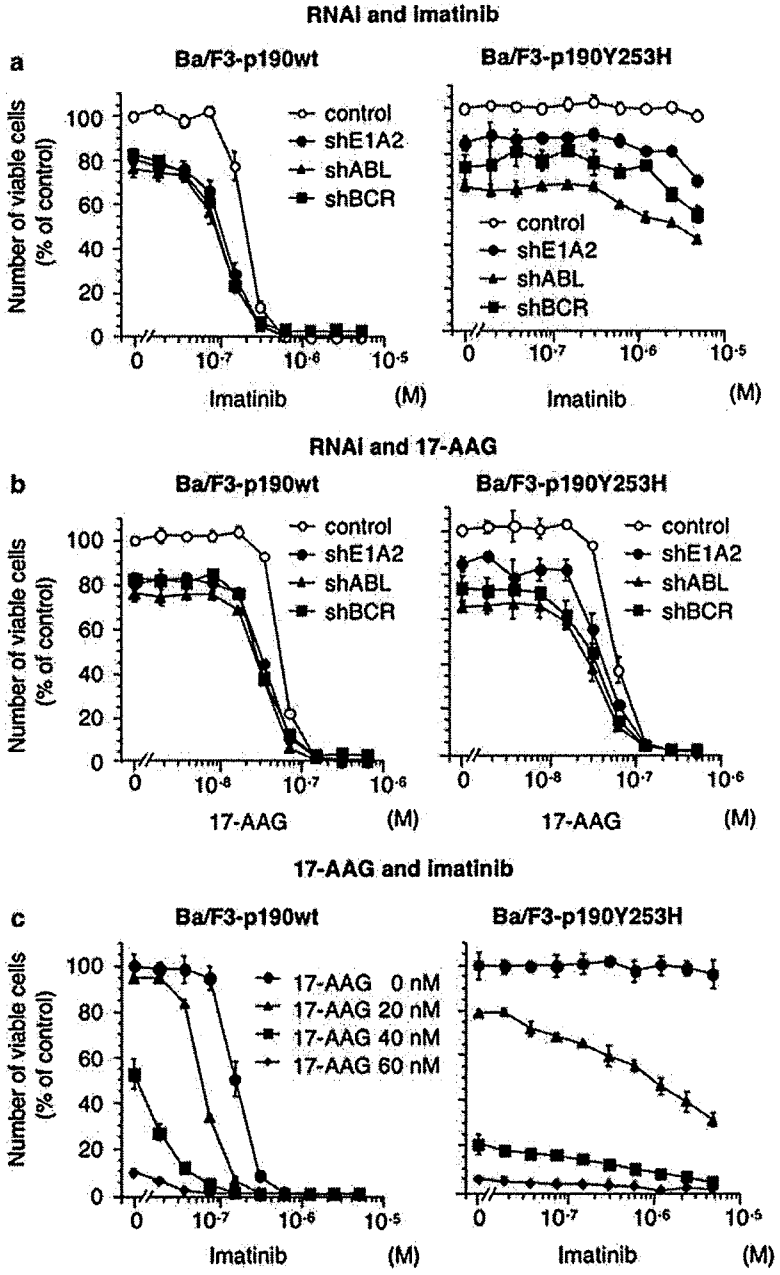

Figure 6 Cell proliferation assay conducted after combined treatment with shRNAs and imatinib or 17-AAG. (a) Combination of shRNAs and imatinib. Ba/F3-p190wt and Ba/F3-p190Y253H cells were transduced with shRNA lentiviral vectors under suboptimal condition (MOI = 1) and cultured in the presence or absence of imatinib (0–5 μM). (b) Combination of shRNAs and 17-AAG. Ba/F3-p190wt cells and Ba/F3-p190Y253H cells were transduced with shRNA lentiviral vectors at an MOI of 1 and cultured in the presence or absence of 17-AAG (0–500 nM). (c) Combination of 17-AAG and imatinib. Ba/F3-p190wt cells and Ba/F3-p190Y253H cells were treated with various combinations of 17-AAG (0–60 nM) and imatinib (0–5 μM). Viable cell number was determined using a WST-8 assay after the 96 h of treatment.

rescued by exogenous IL-3, indicating that neither Abl nor Bcr is essential for response to IL-3. In addition, shABL, but not shBCR, inhibited CFU-GEMM/BFU-E-derived colony formation, which suggests that Abl plays a role especially in normal erythropoiesis. Furthermore, shABL, but not shBCR, profoundly depleted 293 cells during the culture of several days, suggesting the tissue-specific critical role of Abl (data not shown). Thus, it is possible that, with an improved delivery system such as our previously developed CD19-targeted liposomes,[23] anti-p190 shRNAs may become a therapeutic option in Ph$^+$ ALL.

Hsp90 is a molecular chaperon that forms complexes with a variety of polypeptides and facilitates the initial folding and stabilization of its client proteins. Hsp90 is disrupted by 17-AAG,[24] which induces the degradation of p190/p210[18,19] and thereby inhibits the proliferation of p190/p210$^+$ cells with or without the kinase domain mutation.[25] We revealed that 17-AAG downregulated p190 and other signaling molecules downstream of p190. Some studies have shown that anti-p210 siRNA in combination with imatinib or 17-AAG exerts more potent activity than control siRNA with imatinib or 17-AAG in

p210$^+$ cells, with or without the kinase domain mutation.[12,26] In addition, Radujkovic *et al.*[27] have shown that combination treatment with 17-AAG and imatinib inhibits cell proliferation additively/antagonistically in imatinib-sensitive p210$^+$ cells and synergistically in imatinib-resistant cells. Our results are closely compatible with these data, and combination-targeting strategies, as described here, may have enhanced therapeutic potency.

The activation of Stat5 in Ph$^+$ leukemia cells is well recognized,[28,29] but its significance in the pathogenesis of Ph$^+$ leukemia is controversial. However, BCR-ABL-transduced hematopoietic progenitors from Stat5-null mice cannot generate leukemia in recipient mice,[30] and that anti-Stat5 siRNA impairs Ph$^+$ myeloid colony formation in CML.[31] These two recent studies suggest that Stat5 contributes to Bcr-Abl-induced leukemogenesis. Bcr-Abl may directly activate Stat5 through phosphorylation,[32,33] or may indirectly activate Stat5 through phosphorylation by Jak2 or Src family kinases,[28,34,35] both of which are activated in Bcr-Abl-expressing cells. Interestingly, tyrosine phosphorylation of Stat5 was substantially eliminated in BaF/3-p190wt cells transduced with anti-p190 shRNAs, whereas Jak2, Akt and MEK1/2 were still in an activated state. These results offer further evidence for the critical role of Stat5 in Bcr-Abl-induced transformation of hematopoietic cells. It is likely that p190 directly phosphorylates Stat5 and that Jak2 is remote from activation of Stat5 in this cell context, although the possible involvement of Src family kinases such as Hck and Lyn cannot be excluded. The mechanism by which phophorylation of several signal transducers was maintained after p190 down-regulation remains to be elucidated. Nevertheless, compared with the PI3K/Akt and Ras/Raf/MEK/ERK pathways, the Stat5 signaling pathway contributes more closely to p190-mediated transformation of hematopoietic cells.

In conclusion, RNAi-mediated silencing of p190 is a promising tool for both signal transduction delineation and therapeutic application in p190-expressing leukemia.

Acknowledgements

We thank Dr IM Verma (Salk Institute, La Jolla, CA, USA) and Cell Genesys for providing HIV vector constructs. We are indebted to Mr K Takahashi, Ms S Suzuki and Ms M Oiwa for technical support.

References

1 Lugo TG, Pendergast AM, Muller AJ, Witte ON. Tyrosine kinase activity and transformation potency of bcr-abl oncogene products. *Science* 1990; **247**: 1079–1082.
2 Melo JV. The diversity of BCR-ABL fusion proteins and their relationship to leukemia phenotype. *Blood* 1996; **88**: 2375–2384.
3 Druker BJ, Tamura S, Buchdunger E, Ohno S, Segal GM, Fanning S *et al.* Effects of a selective inhibitor of the Abl tyrosine kinase on the growth of Bcr-Abl positive cells. *Nat Med* 1996; **2**: 561–566.
4 Weisberg E, Manley PW, Breitenstein W, Bruggen J, Cowan-Jacob SW, Ray A *et al.* Characterization of AMN107, a selective inhibitor of native and mutant Bcr-Abl. *Cancer Cell* 2005; **7**: 129–141.
5 Lombardo LJ, Lee FY, Chen P, Norris D, Barrish JC, Behnia K *et al.* Discovery of N-(2-chloro-6-methyl- phenyl)-2-(6-(4-(2-hydroxyethyl)- piperazin-1-yl)-2-methylpyrimidin-4- ylamino)thiazole-5-carboxamide (BMS-354825), a dual Src/Abl kinase inhibitor with potent antitumor activity in preclinical assays. *J Med Chem* 2004; **47**: 6658–6661.
6 von Bubnoff N, Peschel C, Duyster J. Resistance of Philadelphia-chromosome positive leukemia towards the kinase inhibitor imatinib (STI571, Glivec): a targeted oncoprotein strikes back. *Leukemia* 2003; **17**: 829–838.
7 Deininger M, Buchdunger E, Druker BJ. The development of imatinib as a therapeutic agent for chronic myeloid leukemia. *Blood* 2005; **105**: 2640–2653.
8 Soda Y, Tani K, Bai Y, Saiki M, Chen M, Izawa K *et al.* A novel maxizyme vector targeting a bcr-abl fusion gene induced specific cell death in Philadelphia chromosome-positive acute lymphoblastic leukemia. *Blood* 2004; **104**: 356–363.
9 Elbashir SM, Harborth J, Lendeckel W, Yalcin A, Weber K, Tuschl T. Duplexes of 21-nucleotide RNAs mediate RNA interference in cultured mammalian cells. *Nature* 2001; **411**: 494–498.
10 Hannon GJ. RNA interference. *Nature* 2002; **418**: 244–251.
11 Wilda M, Fuchs U, Wossmann W, Borkhardt A. Killing of leukemic cells with a BCR/ABL fusion gene by RNA interference (RNAi). *Oncogene* 2002; **21**: 5716–5724.
12 Wohlbold L, van der Kuip H, Miething C, Vornlocher HP, Knabbe C, Duyster J *et al.* Inhibition of bcr-abl gene expression by small interfering RNA sensitizes for imatinib mesylate (STI571). *Blood* 2003; **102**: 2236–2239.
13 Li MJ, McMahon R, Snyder DS, Yee JK, Rossi JJ. Specific killing of Ph+ chronic myeloid leukemia cells by a lentiviral vector-delivered anti-bcr/abl small hairpin RNA. *Oligonucleotides* 2003; **13**: 401–409.
14 Scherr M, Battmer K, Schultheis B, Ganser A, Eder M. Stable RNA interference (RNAi) as an option for anti-bcr-abl therapy. *Gene Therapy* 2005; **12**: 12–21.
15 Wohlbold L, van der Kuip H, Moehring A, Granot G, Oren M, Vornlocher HP *et al.* All common p210 and p190 Bcr-abl variants can be targeted by RNA interference. *Leukemia* 2005; **19**: 290–292.
16 Bai Y, Soda Y, Izawa K, Tanabe T, Kang X, Tojo A *et al.* Effective transduction and stable transgene expression in human blood cells by a third-generation lentiviral vector. *Gene Therapy* 2003; **10**: 1446–1457.
17 Steelman LS, Pohnert SC, Shelton JG, Franklin RA, Bertrand FE, McCubrey JA. JAK/STAT, Raf/MEK/ERK, PI3K/Akt and BCR-ABL in cell cycle progression and leukemogenesis. *Leukemia* 2004; **18**: 189–218.
18 Nimmanapalli R, O'Bryan E, Bhalla K. Geldanamycin and its analogue 17-allylamino-17-demethoxygeldanamycin lowers Bcr-Abl levels and induces apoptosis and differentiation of Bcr-Abl-positive human leukemic blasts. *Cancer Res* 2001; **61**: 1799–1804.
19 Nimmanapalli R, O'Bryan E, Huang M, Bali P, Burnette PK, Loughran T *et al.* Molecular characterization and sensitivity of STI-571 (imatinib mesylate, Gleevec)-resistant, Bcr-Abl-positive, human acute leukemia cells to SRC kinase inhibitor PD180970 and 17-allylamino-17-demethoxygeldanamycin. *Cancer Res* 2002; **62**: 5761–5769.
20 Tybulewicz VL, Crawford CE, Jackson PK, Bronson RT, Mulligan RC. Neonatal lethality and lymphopenia in mice with a homozygous disruption of the c-abl proto-oncogene. *Cell* 1991; **65**: 1153–1163.
21 Schwartzberg PL, Stall AM, Hardin JD, Bowdish KS, Humaran T, Boast S *et al.* Mice homozygous for the ablm1 mutation show poor viability and depletion of selected B and T cell populations. *Cell* 1991; **65**: 1165–1175.
22 Voncken JW, van Schaick H, Kaartinen V, Deemer K, Coates T, Landing B *et al.* Increased neutrophil respiratory burst in bcr-null mutants. *Cell* 1995; **80**: 719–728.
23 Harata M, Soda Y, Tani K, Ooi J, Takizawa T, Chen M *et al.* CD19-targeting liposomes containing imatinib efficiently kill Philadelphia chromosome-positive acute lymphoblastic leukemia cells. *Blood* 2004; **104**: 1442–1449.
24 Prodromou C, Roe SM, O'Brien R, Ladbury JE, Piper PW, Pearl LH. Identification and structural characterization of the ATP/ADP-binding site in the Hsp90 molecular chaperone. *Cell* 1997; **90**: 65–75.
25 Gorre ME, Ellwood-Yen K, Chiosis G, Rosen N, Sawyers CL. BCR-ABL point mutants isolated from patients with imatinib mesylate-resistant chronic myeloid leukemia remain sensitive to inhibitors of the BCR-ABL chaperone heat shock protein 90. *Blood* 2002; **100**: 3041–3044.
26 Withey JM, Harvey AJ, Crompton MR. RNA interference targeting of Bcr-Abl increases chronic myeloid leukemia cell killing by 17-allylamino-17-demethoxygeldanamycin. *Leuk Res* 2006; **30**: 553–560.

27 Radujkovic A, Schad M, Topaly J, Veldwijk MR, Laufs S, Schultheis BS *et al.* Synergistic activity of imatinib and 17-AAG in imatinib-resistant CML cells overexpressing BCR-ABL–Inhibition of P-glycoprotein function by 17-AAG. *Leukemia* 2005; **19**: 1198–1206.
28 Shuai K, Halpern J, ten Hoeve J, Rao X, Sawyers CL. Constitutive activation of STAT5 by the BCR-ABL oncogene in chronic myelogenous leukemia. *Oncogene* 1996; **13**: 247–254.
29 Carlesso N, Frank DA, Griffin JD. Tyrosyl phosphorylation and DNA binding activity of signal transducers and activators of transcription (STAT) proteins in hematopoietic cell lines transformed by Bcr/Abl. *J Exp Med* 1996; **183**: 811–820.
30 Hoelbl A, Kovacic B, Kerenyi MA, Simma O, Warsch W, Cui Y *et al.* Clarifying the role of Stat5 in lymphoid development and Abelson-induced transformation. *Blood* 2006; **107**: 4898–4906.
31 Scherr M, Chaturvedi A, Battmer K, Dallmann I, Schultheis B, Ganser A *et al.* Enhanced sensitivity to inhibition of SHP2, STAT5, and Gab2 expression in chronic myeloid leukemia (CML). *Blood* 2006; **107**: 3279–3287.
32 Nieborowska-Skorska M, Wasik MA, Slupianek A, Salomoni P, Kitamura T, Calabretta B *et al.* Signal transducer and activator of transcription (STAT)5 activation by BCR/ABL is dependent on intact Src homology (SH)3 and SH2 domains of BCR/ABL and is required for leukemogenesis. *J Exp Med* 1999; **189**: 1229–1242.
33 Sillaber C, Gesbert F, Frank DA, Sattler M, Griffin sJD. STAT5 activation contributes to growth and viability in Bcr/Abl-transformed cells. *Blood* 2000; **95**: 2118–2125.
34 Wilson-Rawls J, Xie S, Liu J, Laneuville P, Arlinghaus RB. P210 Bcr-Abl interacts with the interleukin 3 receptor beta(c) subunit and constitutively induces its tyrosine phosphorylation. *Cancer Res* 1996; **56**: 3426–3430.
35 Klejman A, Schreiner SJ, Nieborowska-Skorska M, Slupianek A, Wilson M, Smithgall TE *et al.* The Src family kinase Hck couples BCR/ABL to STAT5 activation in myeloid leukemia cells. *EMBO J* 2002; **21**: 5766–5774.

Supplementary Information accompanies the paper on the Leukemia website (http://www.nature.com/leu)

Biochemical and Biophysical Research Communications 369 (2008) 801–806

Contents lists available at ScienceDirect

Biochemical and Biophysical Research Communications

journal homepage: www.elsevier.com/locate/ybbrc

Common marmoset embryonic stem cell can differentiate into cardiomyocytes

Hao Chen [a,b], Fumiyuki Hattori [a,c], Mitsushige Murata [a,b], Weizhen Li [a], Shinsuke Yuasa [a], Takeshi Onizuka [a,b], Kenichiro Shimoji [a,b], Yohei Ohno [a,b], Erika Sasaki [d], Kensuke Kimura [a,b], Daihiko Hakuno [a,b], Motoaki Sano [a], Shinji Makino [a], Satoshi Ogawa [b], Keiichi Fukuda [a,*]

[a] Department of Regenerative Medicine and Advanced Cardiac Therapeutics, Keio University School of Medicine, 35 Shinanomachi, Shinjuku-ku, Tokyo 160-8582, Japan
[b] Division of Cardiology, Department of Medicine, Keio University School of Medicine, 35 Shinanomachi, Shinjuku-ku, Tokyo 160-8582, Japan
[c] Asubio Pharma Co., Ltd., 1-1-1 Wakayamadai, Shimamoto-cho, Mishima-gun, Osaka 618–8513, Japan
[d] Laboratory of Applied Developmental Biology, Marmoset Research Department, Central Institute for Experimental Animals, 1430 Nogawa, Miyamae-ku, Kawasaki, Kanagawa 216-0001, Japan

ARTICLE INFO

Article history:
Received 7 February 2008
Available online 10 March 2008

Keywords:
Embryonic stem cell
Common marmoset
Primate
Monkey
Cardiomyocytes
Differentiation
Characterization
Heart regeneration
Preclinical model

ABSTRACT

Common marmoset monkeys have recently attracted much attention as a primate research model, and are preferred to rhesus and cynomolgus monkeys due to their small bodies, easy handling and efficient breeding. We recently reported the establishment of common marmoset embryonic stem cell (CMESC) lines that could differentiate into three germ layers. Here, we report that our CMESC can also differentiate into cardiomyocytes and investigated their characteristics. After induction, *FOG-2* was expressed, followed by *GATA4* and *Tbx20*, then *Nkx2.5* and *Tbx5*. Spontaneous beating could be detected at days 12–15. Immunofluorescent staining and ultrastructural analyses revealed that they possessed characteristics typical of functional cardiomyocytes. They showed sinus node-like action potentials, and the beating rate was augmented by isoproterenol stimulation. The BrdU incorporation assay revealed that CMESC-derived cardiomyocytes retained a high proliferative potential for up to 24 weeks. We believe that CMESC-derived cardiomyocytes will advance preclinical studies in cardiovascular regenerative medicine.

Cardiomyocytes have been known to terminally differentiate and lose their ability to proliferate soon after birth [1]. Some researchers have reported the possible existence of adult cardiac stem or progenitor cells [2–4], but unfortunately these cells do not have sufficient proliferation ability for repairing the damaged heart [5]. Therefore, once the physical or functional loss of myocytes occurs due to myocardial infarction (MI) or myocarditis, a damaged heart cannot recover its structure and function. The characteristics of embryonic stem (ES) cells include clonal and unlimited expansion, as well as differentiation into various cell types including cardiomyocytes [6]. Thus, human ES cells would be an attractive cell source for regenerative heart therapy. However, before these can be applied clinically, the therapeutic efficacy and safety of ES cell-derived cardiomyocytes must be proven in preclinical experiments using a primate model system.

To date, rhesus and cynomolgus monkeys have been the most frequently used primate models in preclinical studies. Recently, the common marmoset monkey (*Callithrix jacchus*) has attracted a great deal of attention as a potential laboratory and preclinical experimental animal, because it has many advantages including a small body, a short gestation period (approximately 144 days), early sexual maturity (12–18 months), bears 4–6 progeny/year, is cost efficient and is easy to maintain. Recently, we reported the establishment of three CMESC lines, which have many similarities to human ES cells including morphology, surface antigens and cellular characteristics [7]. It is expected that common marmoset monkeys and CMESC-derived differentiated cells will provide a powerful preclinical model for studies in the field of regenerative medicine.

Rhesus and cynomolgus monkey ES cells have already been established [8,9], and these ES cells are able to differentiate into cardiomyocytes [10,11]. We have reported previously that CMESC lines can differentiate into neuron and glia, and induce formation of teratomas including cartilage, adipose tissue, skeletal muscle, a bronchus-like structure, keratinizing squamous epidermis, epidermis and CD31-positive vascular endothelial cells [7]. However, we were not able to induce cardiomyocyte differentiation from CMESC.

To utilize this system for preclinical studies into heart regeneration, we investigated conditions that were suitable for cardiomyocyte induction from CMESC. Here we report the successful

* Corresponding author. Address: Department of Regenerative Medicine and Advanced Cardiac Therapeutics, Keio University School of Medicine, 35 Shinanomachi, Shinjuku-ku, Tokyo 160-8582, Japan. Fax: +81 3 5363 3875.
E-mail address: kfukuda@sc.itc.keio.ac.jp (K. Fukuda).

0006-291X/$ - see front matter © 2008 Elsevier Inc. All rights reserved.
doi:10.1016/j.bbrc.2008.02.141

differentiation of CMESC into cardiomyocytes. The CMESC-derived cardiomyocytes were characterized in detail.

Materials and methods

Common marmoset ES cell culture and differentiation. The CMESC lines No. 20 and 40 were obtained from the Laboratory of Applied Developmental Biology, Marmoset Research Department, Central Institute for Experimental Animals [7]. CMESCs were cultured on 10 μg/mL mitomycin C-treated mouse embryonic fibroblast (MEF) feeder cells with CMESM (common marmoset ES cell medium) culture medium, which consisted of 80% Knockout Dulbecco's modified Eagle's medium (KO-DMEM; Invitrogen Co., 10829-018) supplemented with 20% Knockout Serum Replacement® (KSR; Invitrogen Co., 10828-028), 0.1 mM MEM Non-Essential Amino Acids Solution (Sigma–Aldrich Co., M7145), 2 mM L-Glutamine (Invitrogen Co., 25030-081), 0.1 mM β-Mercaptoethanol (2-ME; Sigma–Aldrich Co., M-7522) and 4 ng/mL basic fibroblast growth factor (bFGF; Wako Pure Chemical Industries Ltd., 064-04541). CMESCs were passaged every 5 or 6 days to maintain them in an undifferentiated state.

For differentiation, CMESC colonies of an appropriate size were chosen using a combination of 40-μm and 100-μm cell-strainers (Becton–Dickinson) that also facilitated the complete removal of feeder cells. Embryoid bodies (EBs) were formed by suspending and culturing colonies in Petri dishes during the first 10 days. To evaluate the incidence of beating EBs, EBs were distributed in non-adhesive 96-well culture plates (Sumitomo Bakelite Co., Ltd.) with approximately 1–2 EBs per well.

Reverse transcription-polymerase chain reaction (RT-PCR) analysis. Total RNA was prepared from EBs using ISOGEN (Nippon gene Co., Ltd., 317-02501), according to the manufacturer's instructions. Contaminating genomic DNA was degraded by RNase-Free DNase I (Ambion, Japan, #2222) at 37 °C for 30 min. Following phenol–chloroform extraction and ethanol precipitation, total RNA was reverse transcribed into cDNA using the Oligo-(dT)12-18 primer (Superscript II RT kit; Invitrogen Co., 18064-022) and then amplified by PCR using RED-Taq DNA polymerase (Sigma–Aldrich Co., D4309). The primer sequences and PCR conditions are listed online in Supplementary Table 1.

Immunofluorescent staining. EBs (6–8 weeks after differentiation) were fixed in 4% paraformaldehyde for 30 min at room temperature, cryoprotected with sucrose and cryosectioned into 7-μm sections. After pretreatment with ImmunoBlock® (Dainippon Sumitomo Pharma Co., Ltd., KN001), the sections were incubated at 4 °C overnight with the primary antibodies diluted in TBST (Tris-buffered saline with 0.1% Tween 20). The fluorescent dye-conjugated secondary antibodies were then applied to the sections for 30 min at 37 °C. The antibodies used in this study are listed online in Supplementary Table 2. The nuclei were stained with DAPI or ToPro-3 (Invitrogen Co.) and observed by conventional fluorescent microscopy (IX71; Olympus Co.) and confocal Laser microscopy (LSM510 META; Carl Zeiss Inc.), respectively.

Transmission electron microscopy (TEM). EBs were fixed in cold 2.5% glutaraldehyde with 2% paraformaldehyde in 0.1 mol/L cacodylate buffer (pH 7.4), post-fixed in 1% osmium tetroxide, dehydrated and embedded in Epon resin. Ultrathin sections were mounted on copper grids, stained with uranyl acetate and lead citrate, and examined by TEM (Philips).

Electrophysiology. The microscope was equipped with a recording chamber and a noise-free heating plate (Microwarm Plate; Kitazato Supply). A 10 mmol/L volume of HEPES was added to the culture medium to maintain the pH of the perfusate at 7.5–7.6. Standard glass microelectrodes that had a DC resistance of 25–35 MΩ when filled with pipette solution (2 mol/L KCl) were used. The electrodes were positioned using a motor-driven micromanipulator (EMM-3SV; Narishige) under optical control. Spontaneously beating cells were selected as targets, and the action potentials of the targeted cells were recorded. The recording pipette was connected to a patch-clamp amplifier (Axopatch 200B; Axon Instruments), and the signal was passed through a low-pass filter with a cut-off frequency of 2 kHz and digitized with an A/D converter with a sampling frequency of 10 kHz (Digidata 1440A; Axon Instruments). Signals were monitored, recorded as electronic files, and analyzed offline with pCLAMP 10 software (Axon Instruments).

BrdU incorporation assay. After three weeks of differentiation, the medium was changed and EBs were cultured in α-MEM supplemented with 10% FCS. Five to 36-week-old EBs were divided into two groups. EBs in Group 1 (intact EB) were cultured with 10 μmol/L of BrdU for 24 h in α-MEM supplemented with 10% FCS, then fixed with 4% paraformaldehyde. After treatment with 20% sucrose for 1 hour at RT, the fixed cells were cryosectioned. The sections were immersed in 2 N HCl with 0.5% Tween 20 solution for 20 min. Cardiomyocytes that had incorporated BrdU were detected using the BrdU Labeling and Detection Kit I (Roche Diagnostics Co., 11296736001) according to the manufacturer's instructions, except that the primary antibody for Nkx2.5 and the secondary antibody conjugated with Alexa-546 (Invitrogen Co.) were also used to identify cardiomyocytes. EBs in Group 2 (dispersed condition) were dispersed by 0.1% trypsin and 0.1% collagenase type III (Worthington Biochemical Co., #4182) in ADS buffer (116 mM NaCl, 20 mM HEPES, 12.5 mM NaH_2PO_4, 5.6 mM glucose, 5.4 mM KCl, and 0.8 mM $MgSO_4$, pH 7.35) with stirring. After 2 days of culture in α-MEM supplemented with 10% FCS, 10 μmol/L of BrdU was added and the dispersed EBs were cultured for a further 24 h at 37 °C in the same medium. Detection of BrdU-incorporated cardiomyocytes was performed as described above.

Results

Differentiation of CMESCs into spontaneously contracting cardiomyocytes

The two lines of CMESCs were cultured in medium containing KSR instead of animal-derived serum in order to maintain pluripotency (Fig. 1A, left). To stimulate the CMESCs to differentiate into cardiomyocytes, we adopted a conventional floating culture system and tested several combinations of medium (DMEM, KO-DMEM or α-MEM) and several lots of fetal calf serum (FCS) or KSR. We succeeded in stimulating CMESC line No. 20 to differentiate into contracting EBs, but failed to differentiate CMESC line No.40 under all conditions tested. CMESC line No. 20 could differentiate into EBs with contracting areas when a combination of three out of five lots of FCS (5–20% in use) and KO-DMEM or α-MEM were used. Strikingly, beating EBs could be obtained very efficiently by culturing the cells in KO-DMEM supplemented with 20% KSR, which was named dCMESM (common marmoset ES cell medium for cardiomyocyte differentiation). This had the same composition as the CMESM, but lacked bFGF. Confluent cultures of undifferentiated CMESCs were completely dissociated from the feeder cells and cultured in suspension to form EBs in dCMESM. In the floating culture system, CMESCs efficiently developed EBs and spontaneously beating cells (Supplementary Movie). An average of 10–20% of EBs began spontaneously contracting 12–15 days after differentiation. A maximum percentage (46 ± 13%) of contractile EBs was observed at approximately 18 days after differentiation, and was roughly sustained for two months.

Most contractile areas within EBs were located in the cell mass or the periphery of cystic structures. Contraction of CMESC-derived EBs was highly sensitive to temperature, a characteristic shared by human ES-derived EBs. EBs were cryosectioned 6–8 weeks after differentiation and immunofluorescent staining was performed. Typically Nkx2.5 and α-Actinin double-positive areas existed in the subsurface of EBs (Fig. 1A, center and right). In the cardiomyocyte-containing EBs, the Nkx2.5 and α-Actinin double-positive cells were approximately 30% of total cells.

Immunofluorescent staining and microstructure of CMESC-derived cardiomyocytes

Immunofluorescent staining was essential to determine the cardiomyocyte structure and the expression of cardiomyocyte-specific proteins. However, at the start of this study, the type of antibodies that would recognize common marmoset monkey cardiomyocytes was unknown. We therefore tested various antibodies that could detect cardiomyocyte-specific proteins in the CMESC-derived cardiomyocytes. Spontaneously beating EBs were dispersed and the CMESC-derived cardiomyocytes were cultured under adherent culture conditions. Immunofluorescent staining was then performed. Antibodies for the cardiac-specific transcription factors Nkx2.5 and GATA4 strongly labeled the nuclei of the CMESC-derived cardiomyocytes. Moreover, antibodies for α-Actinin, myosin heavy chain (MHC), myosin light chain (MLC) and Tropomyosin strongly labeled the typical myofilament structure of the cardiomyocytes. The antibody for the atrial natriuretic peptide (ANP) highlighted the secretary granules typical of cardiomyocytes surrounding the nucleus (Fig. 1B).

Microstructural analysis using TEM revealed typical myofilament structures, desmosomes and a number of mitochondria in CMESC-derived cardiomyocytes (Fig. 1C).

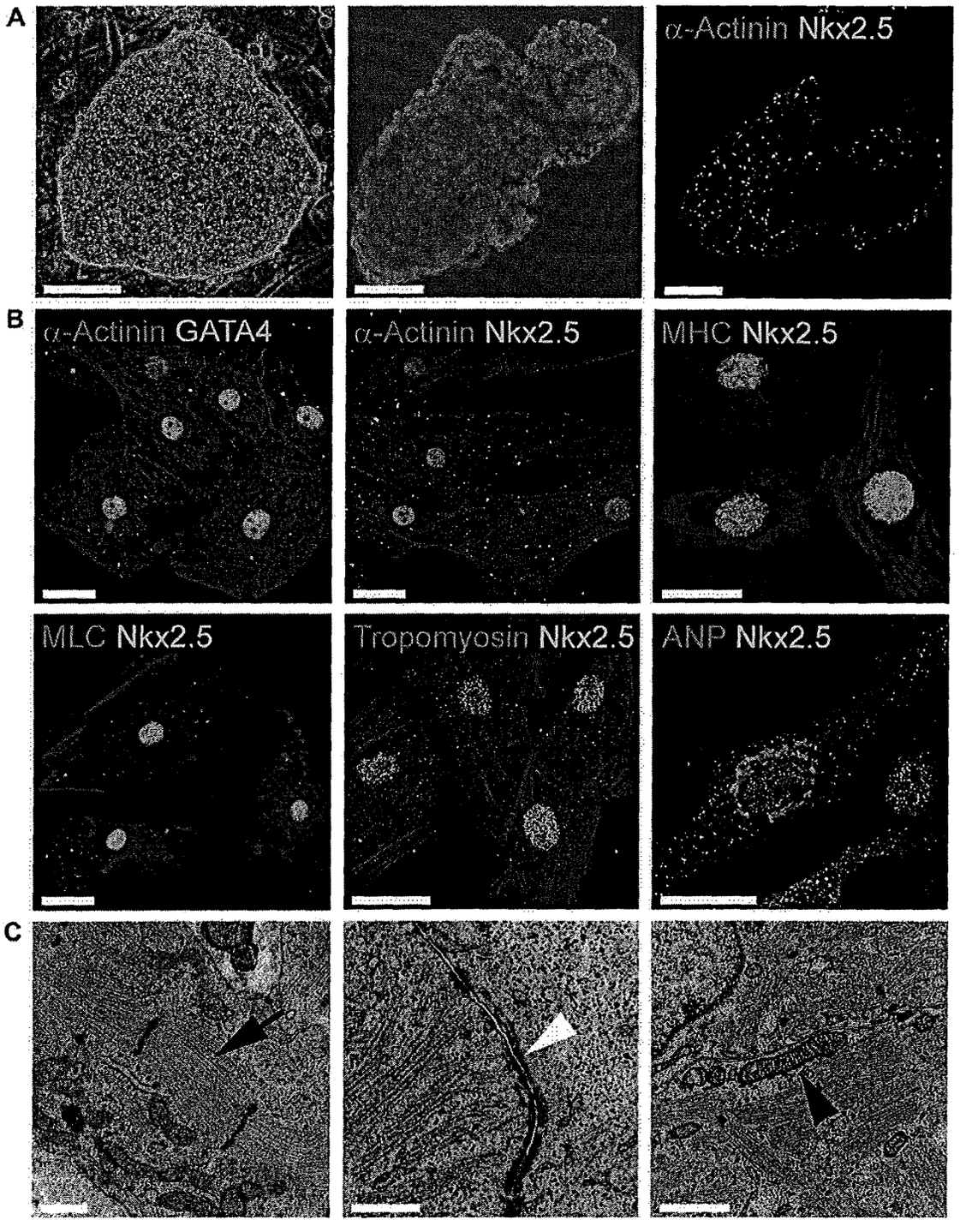

Fig. 1. Structural studies of CMESC-derived cardiomyocytes. (A) Phase contrast microscopy of the undifferentiated CMESC (left), and typical cardiomyocyte-containing non-cystic embryoid body (EB) (center). Immunofluorescent microscopy of cryosections of EBs using anti-α-Actinin and Nkx2.5 antibodies. (B) Double immunofluorescent staining for Nkx2.5 or GATA4 combined with α-Actinin, MHC, MLC, Tropomyosin or ANP. (C) Transmission electron microscopy of the CMESC-derived cardiomyocytes: striated muscle fiber (left, black arrow), desmosomal structure (middle, white arrow head) and mitochondria (right, black arrow head). Scale bars: (A) 100 μm; (B), 20 μm; (C) 0.5 μm.

Time course of marker gene expression during cardiomyocyte differentiation

To characterize the differentiation pathway of undifferentiated CMESC into cardiomyocytes, we performed semi-quantitative RT-PCR to analyze the expression of various marker genes associated with pluripotency, visceral endoderm, and early and late cardiomyogenesis. Some of the primers used have been described previously [7,10], and some were designed based on similar murine, *macaca fascicularis* and *homo sapiens* sequences (Supplementary Table 1). The pluripotency markers *Nanog* and octamer-binding transcription factor 3 (*Oct3/4*) were expressed at high levels in

undifferentiated ES cells. Expression levels of both markers gradually decreased upon differentiation and completely disappeared at day 15 post-differentiation (Fig. 2A). The early mesendoderm marker *Brachyury* was observed from day 3 post-differentiation, peaked at day 6 post-differentiation, but could not be detected at day 9 post-differentiation (Fig. 2B). The visceral endoderm marker alpha-fetoprotein (*AFP*) was observed from day 3 post-differentiation and peaked at day 9 post-differentiation, but could not be detected at day 15 post-differentiation (Fig. 2C). For the genes encoding cardiac-related transcription factors, the expression of the friend of GATA 2 (*FOG-2*) was first observed from day 3 post-differentiation, *GATA4* and the t-box 20 (*Tbx-20*) were from day 6 post-differentiation, *Tbx5* was from day 9 post-differentiation, and *Nkx2.5* was strongly observed at day 15 post-differentiation (Fig. 2D). For the cardiomyocyte-specific proteins, *ANP* and the MLC 2 atrial (*MLC2a*) were observed first from day 6 post-differentiation, *α-MHC* and *β-MHC* were from day 9 post-differentiation, the MLC 2 ventricular (*MLC2v*) was from day 12 post-differentiation (Fig. 2E).

Action potential recordings of CMESC-derived cardiomyocytes

We recorded the action potentials of CMESC-derived cardiomyocytes using glass microelectrodes. Eight-week-old contracting EBs were selected manually and dispersed into small clumps and single cells. The dispersed EBs were cultured to confluence for three days before analysis. The microelectrode was advanced to the intracellular cytoplasm and the voltage of the bulk solution and cytoplasm were measured. Rhythmic beating could be detected in the CMESC-derived cardiomyocytes. The action potential resembled a sinus node, indicating that the CMESC-derived cardiomyocytes had a relatively shallow resting membrane potential, slow diastolic depolarization and relatively long action potential duration (Fig. 3A). The administration of isoproterenol increased their beating rates (Fig. 3B). The basic cycle length (BCL), action potential duration (APD), dV/dt, action potential amplitude (APA) and maximum diastolic potential (MDP) were also recorded (Fig. 3C).

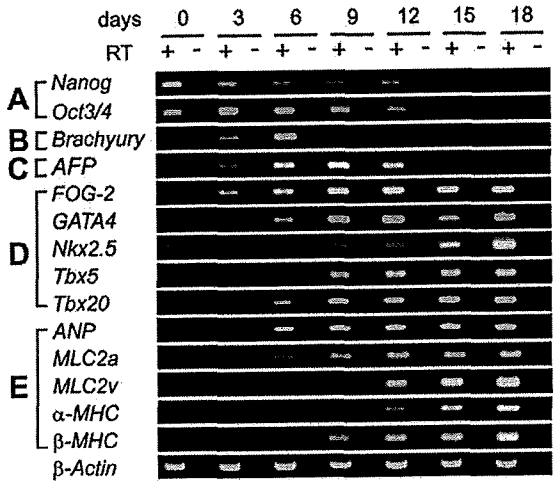

Fig. 2. RT-PCR analysis of the CMESC-derived EBs for various immature and cardiomyocyte-specific proteins. (A) Pluripotency-related genes: *Nanog* and *Oct3/4*; (B) Mesodermal marker gene: *Brachyury*; (C) Primitive endodermal marker gene: *AFP*; (D) cardiomyocyte-precursor and cardiomyocyte marker genes: *FOG-2*, *GATA4*, *Nkx2.5*, *Tbx5*, and *Tbx20*; (E) Cardiomyocyte-associated structural protein genes: *ANP*, *MLC2a*, *MLC2v*, *α-MHC*, *β-MHC*, and equal loading control β-actin. Reverse-transcription negative controls were also amplified and loaded in the lane next to the relevant sample. Abbreviations are listed in Supplementary Table 1.

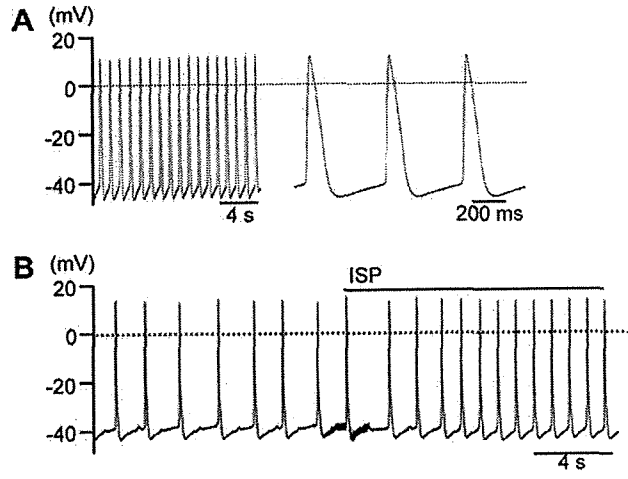

C

BCL (sec)	APD50 (msec)	APD90 (msec)
1.3~3.2	178.1±4.2	316.6±5.8

dV/dt max (V/s)	APA (mV)	MDP (mV)	n
5.6±1.0	68.4±2.5	-45.4±1.8	12

Fig. 3. Electrophysiology of CMESC-derived cardiomyocytes. (A) Representative action potentials of CMESC-derived cardiomyocytes showing spontaneous beating (left) and the relatively short duration time of the action potential (right). (B) Effect of isoproterenol (ISP) on the beating rate. (C) Statistical parameters obtained from 12 cardiomyocytes including beating cycle length (BCL), action potential duration (APD), dV/dt max, action potential amplitude (APA) and maximum diastolic potential (MDP).

Proliferative potential of CMESC-derived cardiomyocytes

Since the gestation period of the common marmoset is approximately seven times longer than that of the mouse, we hypothesized that CMESC-derived cardiomyocytes also retain their proliferative potential for a longer period of time and investigated this possibility. When EBs were dispersed into small clumps we observed a relatively long-term proliferation period and noticeable cell multiplication. From these findings, we expected that CMESC-derived cardiomyocytes might possess a higher proliferation ability than mouse-derived ES cells.

First, we performed BrdU incorporation assays on intact EBs at several time points after differentiation had occurred. The identification of DNA synthesizing cardiomyocytes was confirmed by co-immunofluorescent staining of Nkx2.5 and BrdU. At 6 weeks, intact EBs initially contained 33% BrdU-positive cardiomyocytes, but this decreased to less than 1% at 12 weeks (Fig. 4A and B). Next, the dispersed cells from EBs at several time points were applied to BrdU incorporation assays. Average 73% of cardiomyocytes were positive for BrdU at 5 weeks. This gradually decreased to 30% at 24 weeks, and 0% at 36 weeks (Fig. 4A and C). Most of the cardiomyocytes from freshly dispersed EBs 36 weeks after differentiation were rod-shaped (data not shown). These data indicated that common marmoset ES cell-derived cardiomyocytes retained their proliferation potential for an extended period of time.

Discussion

This is the first study to demonstrate that CMESC can differentiate into cardiomyocytes *in vitro*. We described their overall differentiation mechanism including time-courses for the expression of various genes during cardiogenesis, and characterized them in

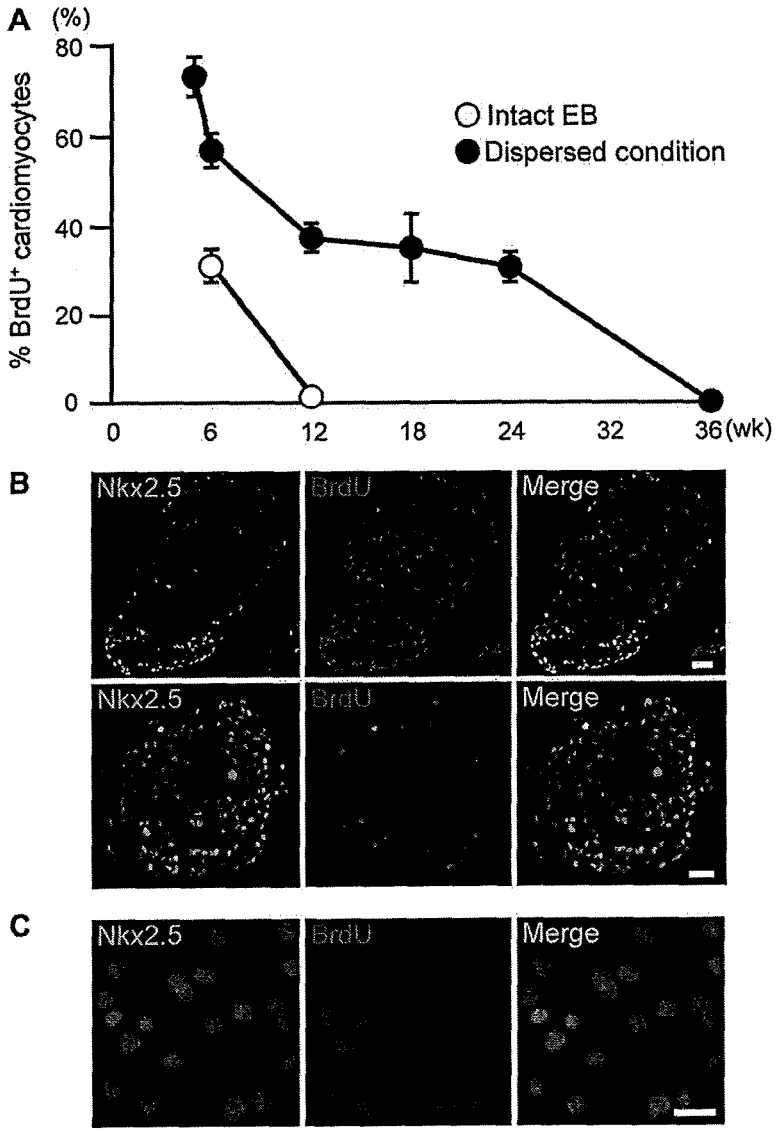

Fig. 4. Proliferation properties of CMESC-derived cardiomyocytes. (A) Time course BrdU incorporation assay in intact EB (open circle; $n = 3$) and dispersed condition (closed circle; $n = 3$) during weeks 5–36 post-differentiation. Cardiomyocytes were identified by immunofluorescent staining for Nkx2.5. The fractions of BrdU-positive cardiomyocytes were plotted. (B) Typical immunofluorescent staining patterns of Nkx2.5 (left), BrdU (middle) and merged images (right) in the intact EBs 6 weeks after differentiation (upper panel) and 12 weeks after differentiation (lower panel). (C) Typical immunodetection of Nkx2.5 (left), BrdU (middle) and merged images (right) in the dispersed condition 6 weeks after differentiation. Scale bars: (B) 100 μm; (C) 20 μm.

detail by immunofluorescent staining, ultrastructural analysis, electrophysiology and determining their growth properties.

Gene expression analyses during cardiogenesis in several species including mice [12], humans [13], and rhesus monkeys [10] are available. The present study enabled us to obtain gene expression data for the common marmoset monkey. A comparison of gene expression profiles between the species listed above highlights many similarities. The only major difference seems be in the timing of cardiomyocyte development: 8–14 days in humans; 12 days in the common marmoset; 8 days in the rhesus monkey; and 6 days in mice. Although minor differences in the expression timings of the *ANP, MLC-2a, MLC-2v* and *α-MHC* genes also exist during differentiation, we found that the timing of CMESCs was closest to human ES cells.

We found that the efficiency of cardiac differentiation was the same when obtained under non-serum conditions using KSR instead of FCS. These observations indicated that CMESCs, unlike human [14] or rhesus monkey [10] ES cells, do not require any serum-derived stimulating factors for mesendoderm induction and cardiogenesis, because KSR does not contain any cytokines or growth factors. On the other hand, the expression of various marker genes during cardiogenesis was very similar to that seen in human [14] and rhesus monkey [10] ES cells, suggesting that CMESCs have a similar cardiogenic differentiation system to human and rhesus monkey ES cells. CMESCs might be able to provide differentiation-inducing auto- and/or paracrine factors. Further mechanistic comparative studies between CMESCs and human and/or rhesus monkey ES cells will provide further insights into cardiogenic differentiation.

BrdU incorporation assay indicated that CMESC-derived cardiomyocytes were capable of long-term proliferation for extended periods of time. Importantly, CMESC-derived cardiomyocytes were still able to proliferate 24 weeks after differentiation, but the ability to proliferate ended at 36 weeks. Considering the gestation

period of the common marmoset, these findings had a reasonable explanation.

Much information about human ES cells and their application to heart regeneration therapy has accumulated [15,16]. Moreover, mouse and human inducible pluripotent stem cells (iPS cell) have also been established [17]. In order for heart regeneration therapy using regenerated cardiomyocytes to become a reality, preclinical studies using primate ES cell- or iPS cell-derived cardiomyocytes for transplantation are necessary. The common marmoset monkey is an ideal primate model for preclinical studies in the field of regenerative medicine. We believe that this report provides fundamental details about CMESC-derived cardiomyocytes that will aid their use as a primate heart cell-therapy model.

Appendix A. Supplementary data

Supplementary data associated with this article can be found, in the online version, at doi:10.1016/j.bbrc.2008.02.141.

References

[1] W.R. MacLellan, M.D. Schneider, Genetic dissection of cardiac growth control pathways, Annu. Rev. Physiol. 62 (2000) 289–319.
[2] B. Dawn, A.B. Stein, K. Urbanek, M. Rota, B. Whang, R. Rastaldo, D. Torella, X.L. Tang, A. Rezazadeh, J. Kajstura, A. Leri, G. Hunt, J. Varma, S.D. Prabhu, P. Anversa, R. Bolli, Cardiac stem cells delivered intravascularly traverse the vessel barrier, regenerate infarcted myocardium, and improve cardiac function, Proc. Natl. Acad. Sci. USA 102 (2005) 3766–3771.
[3] K.L. Laugwitz, A. Moretti, J. Lam, P. Gruber, Y. Chen, S. Woodard, L.Z. Lin, C.L. Cai, M.M. Lu, M. Reth, O. Platoshyn, J.X. Yuan, S. Evans, K.R. Chien, Postnatal isl1+ cardioblasts enter fully differentiated cardiomyocyte lineages, Nature 433 (2005) 647–653.
[4] H. Oh, S.B. Bradfute, T.D. Gallardo, T. Nakamura, V. Gaussin, Y. Mishina, J. Pocius, L.H. Michael, R.R. Behringer, D.J. Garry, M.L. Entman, M.D. Schneider, Cardiac progenitor cells from adult myocardium: homing, differentiation, and fusion after infarction, Proc. Natl. Acad. Sci. USA 100 (2003) 12313–12318.
[5] S. Lyngbaek, M. Schneider, J.L. Hansen, S.P. Sheikh, Cardiac regeneration by resident stem and progenitor cells in the adult heart, Basic Res. Cardiol. 102 (2007) 101–114.
[6] I. Kehat, D. Kenyagin-Karsenti, M. Snir, H. Segev, M. Amit, A. Gepstein, E. Livne, O. Binah, J. Itskovitz-Eldor, L. Gepstein, Human embryonic stem cells can differentiate into myocytes with structural and functional properties of cardiomyocytes, J. Clin. Invest. 108 (2001) 407–414.
[7] E. Sasaki, K. Hanazawa, R. Kurita, A. Akatsuka, T. Yoshizaki, H. Ishii, Y. Tanioka, Y. Ohnishi, H. Suemizu, A. Sugawara, N. Tamaoki, K. Izawa, Y. Nakazaki, H. Hamada, H. Suemori, S. Asano, N. Nakatsuji, H. Okano, K. Tani, Establishment of novel embryonic stem cell lines derived from the common marmoset (Callithrix jacchus), Stem Cells 23 (2005) 1304–1313.
[8] J.A. Thomson, J. Kalishman, T.G. Golos, M. Durning, C.P. Harris, R.A. Becker, J.P. Hearn, Isolation of a primate embryonic stem cell line, Proc. Natl. Acad. Sci. USA 92 (1995) 7844–7848.
[9] H. Suemori, T. Tada, R. Torii, Y. Hosoi, K. Kobayashi, H. Imahie, Y. Kondo, A. Iritani, N. Nakatsuji, Establishment of embryonic stem cell lines from cynomolgus monkey blastocysts produced by IVF or ICSI, Dev. Dyn. 222 (2001) 273–279.
[10] K. Schwanke, S. Wunderlich, M. Reppel, M.E. Winkler, M. Matzkies, S. Groos, J. Itskovitz-Eldor, A.R. Simon, J. Hescheler, A. Haverich, U. Martin, Generation and characterization of functional cardiomyocytes from rhesus monkey embryonic stem cells, Stem Cells 24 (2006) 1423–1432.
[11] M. Hosseinkhani, K. Hasegawa, K. Ono, T. Kawamura, T. Takaya, T. Morimoto, H. Wada, A. Shimatsu, S.G. Prat, H. Suemori, N. Nakatsuji, T. Kita, Trichostatin A induces myocardial differentiation of monkey ES cells, Biochem. Biophys. Res. Commun. 356 (2007) 386–391.
[12] K.R. Boheler, J. Czyz, D. Tweedie, H.T. Yang, S.V. Anisimov, A.M. Wobus, Differentiation of pluripotent embryonic stem cells into cardiomyocytes, Circ. Res. 91 (2002) 189–201.
[13] A. Beqqali, J. Kloots, D. Ward-van Oostwaard, C. Mummery, R. Passier, Genome-wide transcriptional profiling of human embryonic stem cells differentiating to cardiomyocytes, Stem Cells 24 (2006) 1956–1967.
[14] E. Bettiol, L. Sartiani, L. Chicha, K.H. Krause, E. Cerbai, M.E. Jaconi, Fetal bovine serum enables cardiac differentiation of human embryonic stem cells, Differentiation 75 (2007) 669–681.
[15] O. Caspi, I. Huber, I. Kehat, M. Habib, G. Arbel, A. Gepstein, L. Yankelson, D. Aronson, R. Beyar, L. Gepstein, Transplantation of human embryonic stem cell-derived cardiomyocytes improves myocardial performance in infarcted rat hearts, J. Am. Coll. Cardiol. 50 (2007) 1884–1893.
[16] M.A. Laflamme, K.Y. Chen, A.V. Naumova, V. Muskheli, J.A. Fugate, S.K. Dupras, H. Reinecke, C. Xu, M. Hassanipour, S. Police, C. O'Sullivan, L. Collins, Y. Chen, E. Minami, E.A. Gill, S. Ueno, C. Yuan, J. Gold, C.E. Murry, Cardiomyocytes derived from human embryonic stem cells in pro-survival factors enhance function of infarcted rat hearts, Nat. Biotechnol. 25 (2007) 1015–1024.
[17] K. Takahashi, S. Yamanaka, Induction of pluripotent stem cells from mouse embryonic and adult fibroblast cultures by defined factors, Cell 126 (2006) 663–676.

Tohoku J. Exp. Med., 2008, **215**, 167-180

Comparison of 30 Immunity-Related Genes from the Common Marmoset with Orthologues from Human and Mouse

KAZUYOSHI KOHU,[1,*] EIJI YAMABE,[1,*] AYAKO MATSUZAWA,[1] DAISUKE ONDA,[1] HIROSHI SUEMIZU,[2] ERIKA SASAKI,[2] YOSHIKUNI TANIOKA,[2] HIDEO YAGITA,[3] DAISUKE SUZUKI,[4] YOSHIE KAMETANI,[4] TOSHIYUKI TAKAI,[5] ATSUSHI TOYODA,[6] SONOKO HABU[4] and MASANOBU SATAKE[1]

[1]Department of Molecular Immunology, Institute of Development, Aging and Cancer, Tohoku University, Sendai, Japan
[2]Central Institute for Experimental Animals, Kawasaki, Japan
[3]Department of Immunology, Juntendo University School of Medicine, Tokyo, Japan
[4]Department of Immunology, Tokai University School of Medicine, Isehara, Japan
[5]Department of Experimental Immunology, Institute of Development, Aging and Cancer, Tohoku University, Sendai, Japan
[6]RIKEN Genomic Sciences Center, Yokohama, Japan

In the evolution of primates, the common marmoset belongs to the new world monkey family and is distinct from the great ape family (which includes humans). In this study, we predicted the amino acid sequences of 30 immunity-related genes from the common marmoset and compared them with those from human and mouse. The domain composition of each orthologous protein was analyzed by the SMART tool and was found to be the same among the three species. A BLAST search revealed that the common marmoset and human proteins were 86% identical on average, whereas the conservation between the common marmoset and mouse or between the human and mouse was only 60%. This indicates that the common marmoset and human proteins are closely related and are similarly divergent from the mouse. We divided the 30 proteins into two categories based on the degree of conservation between the common marmoset and mouse amino acid sequences. One group included 19 proteins and had a relatively high level of conservation (68% identical), whereas the other 11 proteins were less conserved (45% identical). This suggests that these immunity-related genes do not evolve at a uniform rate. Interestingly, however, ligand/receptor pairs such as interleukin-6 and interleukin-6 receptor appear to have evolved simultaneously. ——— common marmoset; evolution; immunity-related genes; orthologues; cDNA.

Tohoku J. Exp. Med., 2008, **215** (2), 167-180.

Received April 3, 2008; revision accepted for publication April 14, 2008.

Correspondence: Masanobu Satake, M.D., Department of Molecular Immunology, Institute of Development, Aging and Cancer, Tohoku University, Seiryo-machi 4-1, Aoba-ku, Sendai 980-8575, Japan.
e-mail: satake@idac.tohoku.ac.jp
*K.K. and E.Y. contributed to the work equally.

In experimental immunology, the mouse is an outstanding laboratory model organism for a variety of reasons. Mice, like humans, are mammals and therefore observations obtained in mice can be extrapolated to humans. Moreover, several genetically identical mouse strains, such as C57Black/6 and Balb/c, have been established and gene manipulations can be made to generate transgenic or knockout lines. Mice are also advantageous because they can be maintained in a specific pathogen-free or completely germ-free environment.

Despite their similarities, mice and humans belong to different orders (rodents and primates, respectively). This difference is not negligible and can be an issue in several immunological reactions (Mestas and Hughes 2004). For example, the interleukin (IL)2/IL2 receptor system induces T lymphocyte proliferation through the same signaling pathway in both humans and mice. Although human IL2 can bind to both human and murine IL2 receptors with a similar affinity, murine IL2 cannot bind to the human IL2 receptor (Gillis et al. 1978). Such murine- or human-specific ligand-receptor interactions have been also observed for other cytokines and interleukins. Immunologists also encounter species-specificity issues when they use antibodies in experiments. For example, most of the available anti-murine CD4 monoclonal antibodies do not recognize human CD4, and vice versa, anti-human CD4 antibodies do not usually recognize murine CD4. Species-specific antibodies are also available for other CD molecules. The species-specificity in ligand-receptor interactions and monoclonal antibodies reflects the difference in the amino acid sequence of homologous proteins between mice and humans.

Callithrix jacchus (the common marmoset) is a primate model organism (Mansfield 2003). It has several experimental advantages when compared to other nonhuman primates such as its ability to easily breed in a laboratory setting. It does not transmit hazardous infectious agents and has a mild behavior. The common marmoset has become increasingly used in biomedical research in areas such as neuroscience, behavioral research, toxicology and drug development and infectious diseases.

From an evolutionary standpoint of primates, the common marmoset appears to occupy a unique position because it is a new world monkey, distinct from humans and chimpanzees. However, both the common marmoset and human belong to the same anthropoidea suborder of primates. At the upper level, primates (common marmoset and human) constitute one order distinct from that of rodents (mouse). Thus, common marmoset is expected to serve as a milestone to evaluate an evolutional distance of immunity between human and mouse. To gain an insight in such comparative immunology, we have identified and sequenced 30 prominent immunity-related *C. jacchus* genes. We have compared the predicted amino acid sequence of these genes in the common marmoset with those of mouse and human and discuss their evolutional significance.

Materials and Methods

RNA isolation

The thymus and spleen of *C. jacchus* was homogenized in Trizol reagent (Invitrogen Carlsbad, CA, USA), and RNA was extracted with chloroform. The RNA in the aqueous phase was precipitated with isopropanol and washed with ethanol. The RNA pellet was dissolved in RNase-free water and treated with RQ1 RNase-free DNase. The RNA was then mixed with phenol/chloroform and recovered by ethanol precipitation. The pellet was resuspended in RNase-free water.

cDNA synthesis and sequencing

cDNA was synthesized from 5 μg RNA using the Super Script First-Strand Synthesis System (Invitrogen). PCR was performed using LA-Taq polymerase (Takara Ohtsu) and 100 ng cDNA as a template. Each reaction consisted of 30 cycles. Every cycle contained a denaturation step at 94°C for 30 sec, an annealing step at an appropriate temperature (45 to 72°C) for 60 sec and an extension step at 72°C for 60 sec. The sequences of the forward and reverse primers used are listed in Supplementary Table 1. These primers were designed in regions where a high degree of homology between the human and mouse sequences exist. Each PCR product was run on an agarose gel and a band of the correct size was extracted from the gel and cloned in a pGEM-T vec-

tor using the TA-cloning kit (Promega Madison, WI, USA). The cDNA insert was sequenced by the dideoxy-dye-terminator method.

Forward and reverse primers were created so that the length of the amplified product was approximately 500 nucleotides. For each gene of interest, five cDNA clones were isolated and sequenced. If any discrepancies between the sequences for a particular nucleic acid position arose, the nucleic acid most often found in that position was assigned to the final sequence. If the length of the cDNA was expected to be more than 500 nucleotides, multiple pairs of primers were designed to cover its entire length. The overlapping sequences were then assembled into a contiguous sequence.

Sequence analyses

The BLAST and SMART tools were used for the homology and domain analyses, respectively (Marchler-Bauer et al. 2005; Letunic et al. 2006). The three dimensional structure of protein was predicted, using the PDFAMS (Ogata and Ueyama 2000). The student's *t*-test was employed for statistical analyses.

Results and Discusssion

We have chosen 30 immunity-related genes to study in *C. jacchus* (Table 1; Note that *CD4, CD40LG, IGHG, IFNG* and *FASLG* were not included in this study, since these sequences had been deposited at GenBank/NCBI by other groups). The chosen genes encode both membrane proteins and soluble factors. The cDNA sequence for each gene was determined in order to deduce the amino acid sequence of the open reading frame. Each sequence was registered at GenBank/NCBI and the accession number of each gene is shown in Table 1. As for *IGHM (immunoglobulin heavy chain, mu, constant region)* and *IGHE (immunoglobulin heavy chain, epsilon, constant region)*, we determined the sequences that corresponded to a constant region of the molecule but did not contain its variable portion. Since these two cDNA were partial, we did not register their sequences to the database.

The number of amino acids and the domain identity are conserved

The number of amino acid residues in each protein was calculated based on the nucleic acid sequence (Table 1) and was found to be nearly identical between the common marmoset, human and mouse (see Supplementary Table 2). We also surveyed the domain architecture of each common marmoset protein by using the SMART and BLAST (PFAM) programs (Marchler-Bauer et al. 2005; Letunic et al. 2006). The domain identity for each common marmoset protein was identical with its orthologous human and murine proteins (compare the domain composition shown in Table 1 with that in Supplementary Table 2). These findings suggest that the putative functions of the 30 common marmoset proteins examined are identical or similar with the known functions of their homologous human and murine proteins.

Amino acid sequence conservation

We next compared the amino acid sequence homology of the 30 proteins in the common marmoset, human and mouse. For each protein, the percentage of conserved amino acid residues between any two species was calculated. The degree of amino acid conservation between the common marmoset and human proteins ranged from 74% (CD86) to 98% (FCER1G, Fc IgE receptor gamma polypeptide) (Table 1) and the average for the 30 proteins examined was 86% (Table 2). In contrast, the average percentage of amino acid conservation between the common marmoset and the mouse was 60% whereas the human and mouse were 61% conserved. These percentages were significantly less than the 86% observed between common marmosets and humans ($p < 0.001$, by a student t-test). Therefore, the common marmoset and human proteins are relatively close and have diverged from the mouse at approximately the same point.

Analysis of CD8A

To exemplify the above claim, we analyzed the amino acid sequence of CD8A in the three species in further detail. The amino acid sequence of CD8A between the common marmoset and human was 84% conserved, whereas between the common marmoset and mouse and between the human and mouse it was 43% and 40% conserved, respectively (Table 1). Fig. 1A shows the

TABLE 1. Structural features of 30 immunity-related *C. jacchus* genes.

Gene symbol	Accession No.	No. of amino acid residues	Domain composition	Identical aa residues (%)		
				marmoset vs human	marmoset vs mouse	human vs mouse
CD80	EF534214	282	Ig/Ig-like/TM	84	40	40
*IL4**	EF493341	151	IL4_13	83	40	44
*IGHE**		425	Ig-like/ Ig-like/ Ig-like/ Ig-like	77	42	42
CD8A	DQ189217	235	Ig/ TM	84	43	40
*IL6**	DQ658153	212	IL6	89	43	41
CD86	EF534211	327	IgV/TM	74	43	48
*IL6R**	DQ826673	468	Ig-like/ FN3/ TM	88	47	46
*FCER1A**	EF534210	257	IgC2/Ig/TM	82	48	48
CD2	EF534206	352	TM	83	49	50
*IL4R**	DQ826671	824	SCOP:d1iarb1/FN3	85	49	52
IL17F	EF613223	163	BLAST:Pfam IL17	83	56	57
*IL2RA**	DQ520834	272	CCP/ CCP/ TM	81	59	61
CD40	DQ189221	274	TNFR/ TNFR/ TNFR/ TNFR/ TM	85	61	58
*IL2**	DQ826674	154	IL2	92	61	62
IL7R	EF534213	459	BLAST:Pfam FN3	88	62	63
IL17A	EF534212	153	BLAST:Pfam IL17	90	63	63
CD28	EF534209	220	Ig-like/TM	85	63	67
IGHM		453	Ig-like/ Ig-like/ Ig-like/ Ig-like	82	64	64
*IL5**	DQ658152	134	PFAM:IL5	83	65	69
CD19	DQ189219	558	Ig/ Ig/ TM	87	66	66
CD3E	DQ189218	198	IgC2/ TM/ ITAM	80	67	64
*IL5RA**	DQ826672	420	BLAST: FN3/ SCOP:d1egja/ TM	89	68	68
IL2RG	EF534208	368	FN3/TM	94	69	70
ITGAX	EF613221	1161	int-alpha/VWA/int-alpha/int-alpha/ intalpha/int-alpha/TM	89	69	70
IL10	DQ658154	178	IL10	89	71	73
TNF	DQ520835	232	TM/TNF	87	72	79
MS4A1	DQ189220	295	PFAM:CD20	92	74	74
IL6ST	DQ859898	915	Pfam: Lep_receptor_Ig/FN3/ FN3/ FN3/ FN3/ FN3/ TM	96	75	76
CD44	EF613222	362	LINK/TM	94	75	78
FCER1G	EF534207	86	TM/ITAM	98	89	88

Domain composition was examined by SMART and BLAST (PFAM) tools. Abbreviations of domains are Ig, immunoglobulin; TM, transmembrane; IgV, immunoglobulin variable; FN3, fibronectin 3; IgC, immunoglobulin constant; CCP, complement control protein; TNFR, tumor necrosis factor receptor; int-alpha, integrin-alpha; VWA, von Villebrand factor type A; TNF, tumor necrosis factor; LINK, hyarulonan-binding; ITAM, immune-tyrosin activation motif. Three way comparisons of each protein was done using a BLAST tool. The values indicate the degree (%) of identical amino acid residues. The genes above and below the inserted line correspond to the diverged and conserved genes, respectively. Also, the genes indicated by artenisks are ligand-receptor pairs such as *IL2* and *IL2RA*, *IL4* and *IL4R*, *IL5* and *IL5RA*, *IL6* and *IL6R*, and *IGHE* and *FCER1A*.

TABLE 2. Categorization of 30 immunity-related *C. jacchus* genes.

Gene category	Identical aa residues (% in average)		
	marmoset vs human	marmoset vs mouse	human vs mouse
The total 30 genes	86 ± 5.5	60 ± 13	61 ± 13
	$p < 0.001$	$p < 0.001$	
The less conserved 11 genes	83 ± 4.3	45 ± 4.8	46 ± 5.5
		$p < 0.001$	$p < 0.001$
The highly conserved 19 genes	88 ± 5.1	68 ± 7.1	69 ± 7.5

The less conseved genes include *CD80, IL4, IGHE, CD8A, IL6, CD86, IL6R, FCER1A, CD2, IL4R* and *IL17F*, whereas the highly conseved genes include the remaining 19 (see the inserted line in Table 1). A significant difference with the indicated p-value (by the student *t*-test) was detected for the bracket-indicated, pairwise comparison.

amino acid alignment and the characteristic motifs/domains found in human CD8A (Leahy et al. 1992) are indicated by bars. These domains include a signal peptide, 9 beta-strands (A to G), 3 complementary determining regions (CDR1 to CDR3), a hinge region, a transmembrane domain and a $p56^{lck}$-binding site. The beta-strands A-C′ and C″-G form beta sheets, whereas the CDRs do not have a rigid structure but rather form loose loops. The beta sheets and CDRs together constitute the immunoglobulin variable (IgV) region. The hinge region connects the IgV and transmembrane domains.

Each motif/domain of CD8A can be classified into three categories based on its degree of conservation/divergence between the three species. In the first category, the transmembrane domain and intracellular $p56^{lck}$-binding site were highly conserved between the three species. This is consistent with the notion that the transmembrane and intracellular domains evolve slowly compared to extracellular domains. The E, F and G strands were also highly conserved between the three species. In the second category, regions in CD8A including the signal sequence, the A, B, C, C′ and D strands and the CDR1 and CDR3 domains were well conserved between the common marmoset and human but distinct from the mouse. Existence and abundance of these secondly categorized motifs/domains is in line with the above described BLAST scores between the three species. The CDR2 was in the third category. The sequences of primates were drastically different from that of mouse (in this sense, the CDR2 resembles the motifs/domains of the second category), and yet those from common marmoset and human were distinct to some extent from each other (in this aspect, the CDR2 is distinct from the motifs/domains of the second category).

We simulated the three dimensional structure of the common marmoset CD8A protein with the prediction tool, PDFAMS (Ogata and Ueyama 2000) using the structure previously determined for the extracellular domain of human CD8A as a template (Leahy et al. 1992). The overall structure of common marmoset CD8A was quite similar to the human and mouse structures (data not shown). Interestingly, despite the divergence of amino acid sequences in this domain, the CDR2 had similar loop-like configurations in both the common marmoset and human (Fig. 1B). In contrast, the loop predicted for mouse CDR2 was strikingly different from the primate structures of CDR2. Thus, the amino acid sequence in the third category can actually exhibit a feature of second category from the aspect of three dimensional structure.

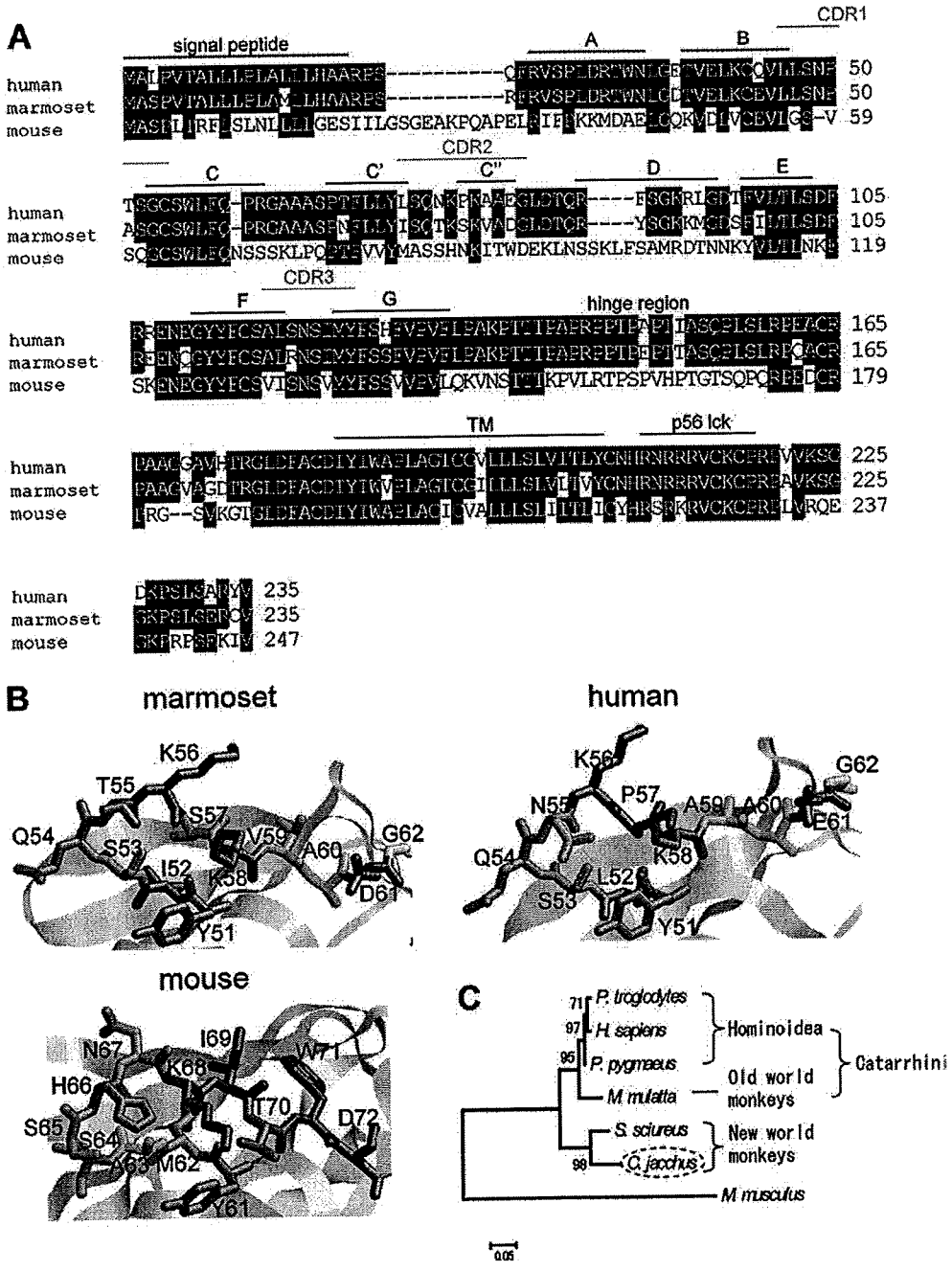
A
signal peptide
CDR1
A
B
human
marmoset
mouse
50
50
59
CDR2
C
C'
C"
D
E
105
105
119
CDR3
F
G
hinge region
165
165
179
TM
p56 lck
225
225
237
235
235
247
B
marmoset
human
mouse
K56
T55
S57
Q54
S53
I52
V59
A60
G62
K58
D61
Y51
N55
P57
A59
A60
E61
L52
C
P. troglodytes
H. sapiens
P. pygmaeus
M. mulatta
S. sciureus
C. jacchus
M. musculus
Hominoidea
Old world monkeys
New world monkeys
Catarrhini
71
97
95
98
0.05